Phase Transition of the El Niño–Southern Oscillation: A Stationary SST Mode

TIANMING LI

Department of Meteorology, Naval Postgraduate School, Naval Research Laboratory, Monterey, California

(Manuscript received 8 April 1996, in final form 23 April 1997)

ABSTRACT

A stationary SST mode is proposed to understand the physical mechanisms responsible for the phase transition of the El Niño–Southern Oscillation. This stationary SST mode differs from the original delayed oscillator mode and the slow SST mode in the sense that it considers both balanced and unbalanced thermocline depth variations and does not take into account the zonal propagation of SST. Within this mode, the Walker circulation acts as a positive feedback mechanism to amplify and maintain an existing interannual SST anomaly, whereas the Hadley circulation acts as a negative feedback mechanism that dismisses the original anomaly and causes the phase shift from a warm (cold) to a cold (warm) episode.

The key to the cause of interannual oscillations in the stationary SST mode lies in the zonal-mean thermocline depth variation that is not in equilibrium with the winds. Because of the nonequilibrium, this part of the thermocline depth anomaly tends to have a phase lag with the wind (or SST) anomaly and therefore holds a key for the interannual oscillation. The zonally asymmetric part of the thermocline depth anomaly, on the other hand, is always in Sverdrup balance with the winds. Such a phase relationship agrees well with observations and with GCM simulations.

The stationary SST mode strongly depends on the basin width, on the air–sea coupling strength, and on the seasonal-cycle basic state. For a reasonable parameter regime, it depicts an interannual oscillation with a period of 2–7 years. This stationary SST mode is also season dependent: it has a maximum growth rate during the later part of the year and a negative growth rate during the northern spring, which may explain the occurrence of the mature phases of the El Niño in the northern winter and a rapid drop of the lagged correlation of the Southern Oscillation index in the boreal spring.

1. Introduction

Over the last decade there have been considerable observational, theoretical, and modeling studies contributing to the understanding of the El Niño–Southern Oscillation (ENSO) phenomenon [see Philander (1990) for a review]. The key premise of these studies is that the interactions between the atmosphere and ocean can support a number of unstable modes through positive feedback processes and promote a self-sustained oscillation. The original hypothesis was proposed by Bjerknes (1966, 1969) and was based on statistical correlation between the Southern Oscillation and sea surface temperature (SST) anomalies in the Pacific, known as the El Niño. He drew a schematic picture in which the intensification and retreat of equatorial trades both force and are forced by SST variations. Following this idea, a variety of simple, conceptual models have been developed to simulate coupled ocean–atmosphere instabilities (e.g., Lau 1981; McCreary 1983; Philander et al. 1984; Gill 1985; Yamagata 1985; Hirst 1986; Battisti

and Hirst 1989; Xie et al. 1989; Neelin 1991; Wakata and Sarachik 1991; Wang and Weisburg 1994; Wang and Feng 1996).

A great challenge of ENSO studies is to understand mechanisms that determine a transition from a warm (cold) to a cold (warm) episode. The positive feedback mechanisms proposed by Bjerknes, Philander et al., Hirst, and others can magnify and maintain a SST anomaly, but what causes the phase change of the oscillation? A transition from a warm (cold) to a cold (warm) phase requires a negative feedback that dismisses the original anomaly. What is the negative feedback?

A major step toward understanding the oscillatory nature of ENSO is through the successful simulations of interannual variability in coupled ocean–atmosphere models (e.g., McCreary and Anderson 1984; Cane and Zebiak 1985; Anderson and McCreary 1985; Zebiak and Cane 1987; Schopf and Suarez 1988; Suarez and Schopf 1988; Philander et al. 1992; Lau et al. 1992). Using an intermediate coupled model, Zebiak and Cane (1987) successfully simulated an ENSO-like variability. They found that a crucial factor causing the interannual oscillation in their model is the thermocline-depth-related subsurface temperature changes. Using a different model, Schopf and Suarez (1988) demonstrated that the interannual oscillation in the model results from the prop-

Corresponding author address: Dr. Tianming Li, Naval Research Laboratory, 7 Grace Hopper Ave., Monterey, CA 93943.
E-mail: li@nrlmry.navy.mil

agation and reflection of equatorial ocean waves. Those waves carry the previous information and propagate across the basin and cause the delayed response of equatorial ocean to the winds. This mechanism was later referred to as the delayed oscillator mode mechanism (Battisti and Hirst 1989). It emphasizes the importance of the reflection of oceanic waves in the western boundary through which a Rossby wave is transferred into an eastward-propagating Kelvin wave that carries an opposite (relative to the one at the equator) signal and counteracts the original anomaly in the eastern equatorial Pacific.

The period of interannual oscillations in the original delayed-oscillator theory depends on individual oceanic wave speed (Battisti and Hirst 1989). However, there is no explicit observational evidence showing the ocean Kelvin and Rossby waves on this timescale (Li and Clarke 1994). Coupled general circulation model (GCM) experiments by Philander et al. (1992) indicate that the explicit evidence of individual oceanic waves is plentiful at higher frequencies in their model but is absent if data are low-pass filtered to isolate the Southern Oscillation. The results imply that the use of terms such as oceanic Rossby or Kelvin waves in describing low-frequency coupled air–sea fluctuations should be regarded as a poetic metaphor. What actually matters is the so-called ocean memory that measures the extent to which the ocean is in disequilibrium with the winds at a given time. Zebiak and Cane (1987) first noticed from their sensitivity experiments that the zonal-mean thermocline depth anomaly is an important indicator for the subsurface ocean memory. Ocean GCM experiments by Schneider et al. (1995) further confirmed that the key for the ocean memory lies in zonally averaged equatorial heat content. By designing backward and forward time integration methods with prescribed observed wind forcing, they found that the fundamental difference between the two experiments lies in the zonal-mean quantities of equatorial heat content. Although uncoupled, their experiments shed lights on some new aspects of the phase transition of ENSO.

Different from the delayed oscillator mechanism, Neelin (1991) proposed a slow SST mode mechanism in which the ocean waves are totally irrelevant to the oscillation. He defined a so-called fast wave limit regime in which the ocean waves are sufficiently fast compared to the advection timescale of SST so that in the first-order approximation, the oceanic wave dynamics are decoupled from the SST equation and the timescale of oscillation is primarily determined by oceanic mixed-layer processes. In the slow SST mode, the thermocline depth anomaly at the equator is always in equilibrium with the wind stress (a Sverdrup balance) so that there is no delay time between them. In other words, only the part of the thermocline depth anomaly that is in equilibrium with the wind was considered and the non-equilibrium part of the thermocline depth anomaly is missing.

The key cause for interannual oscillations in the slow SST mode is the zonal propagation of SST anomalies. Without the zonal propagation, there is no interannual oscillation. This can be easily understood mathematically. To obtain frequency in a single SST equation, one has to introduce an imaginary part, such as anomalous zonal temperature advection, which is associated with the zonal propagation of SST. (The real part reflects instability.) Physically, suppose initially we have a warm SST anomaly in the eastern Pacific. In response to the SST forcing, anomalous westerly winds in the central Pacific are established, which, in turn, cause the deepening of the thermocline in the east (according to the Sverdrup balance) and increase the SST anomaly there. The complex phase patterns associated with various processes in the SST equation cause different phase-propagation tendencies—some are eastward and others are westward. The net effect of these tendencies make the SST anomaly propagate. Once the SST anomaly moves, say, to the western Pacific, the anomalous wind in the central Pacific changes its direction. This causes the shoaling of the thermocline in the eastern Pacific and promotes a cold episode there. As a result, a phase transition completes.

In reality, the SST anomalies do not show significant zonal propagation. Analyses of a four-dimensional data assimilation set conducted by the Coupled Model Project at the National Centers for Environmental Prediction (NCEP) (see Ji et al. 1995 for detail) indicates that during a recent 10-yr period (1983–92) the interannual SST anomaly exhibits a stationary oscillation feature (Fig. 1a). (Hereafter the four-dimensional assimilation data are referred to as observations since they are derived from real ocean measurements.) Coupled model simulations by Zebiak and Cane (1987) and by Philander et al. (1992) (Fig. 1b) showed a similar feature. In fact, our empirical orthogonal function (EOF) analyses, using the 4D data assimilation set, indicate that the first EOF mode of interannual SST anomaly occupies 80% of its total variance. This suggests that in the lowest order of approximation, the interannual SST mode can be regarded as a stationary oscillation mode. Figure 2 illustrates the zonal structure of the first EOF modes for the SST and wind anomalies at the equator. Note that a maximum SST anomaly is found in the eastern Pacific (around 110°W), whereas a peak for the zonal wind anomaly is in the central Pacific (170°W).

In the slow SST mode, only the part of the thermocline depth variations that is in equilibrium with the winds is considered and the disequilibrium part of thermocline depth variations is not. The former reflects a positive feedback (or a coupled instability), whereas the latter influences the frequency. Analyses of the NCEP 4D assimilation dataset reveal that while the zonally asymmetric part of thermocline depth anomaly (represented by 20°C isotherm) is indeed in equilibrium with the wind (and SST) anomalies, the zonal-mean part of the thermocline depth anomaly is clearly not (Fig. 3).
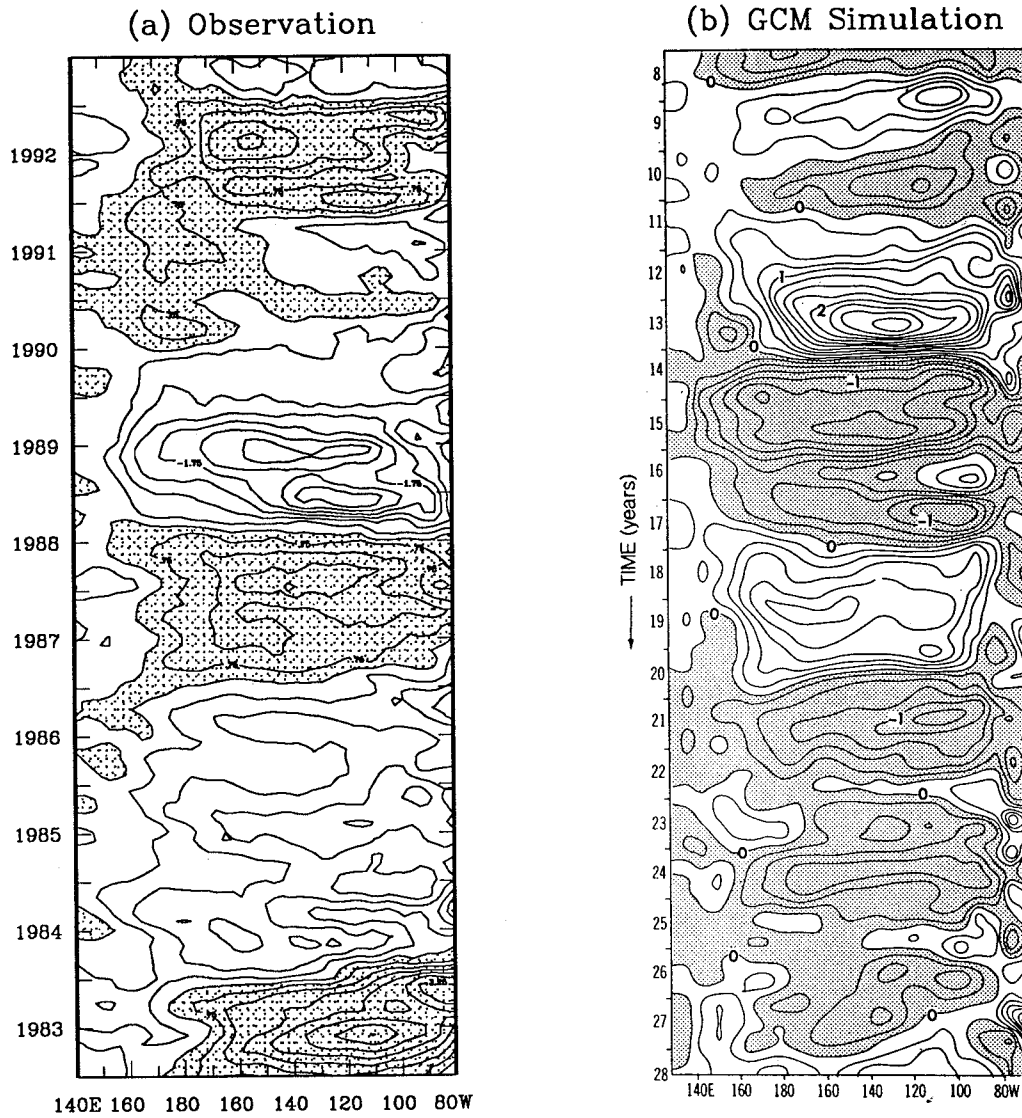
(a) Observation (b) GCM Simulation

FIG. 1. The longitude–time plots of (a) observed and (b) GCM-simulated (Philander et al. 1992) SST anomalies at the equator. The observed data cover a period of July 1982–December 1992. In the left panel the regions of greater than 0.25°C are shaded and the contour interval is 0.5°C. In the right panel negative anomaly regions are shaded and the contour interval is 0.25°C.
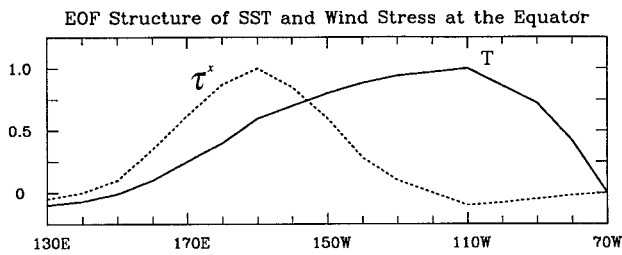

FIG. 2. The zonal profiles of the first EOF mode of interannual SST (the solid line) and zonal wind stress anomalies (the dotted line) along the equator. The EOF analyses are based on the observational dataset from July 1982 to December 1992. Total samples: 126 months and 52 longitude points at the equator.

It follows that a simplest model of ENSO must contain both the balanced and unbalanced parts of the thermocline depth variations.

In this paper, we intend to build a conceptual dynamic model of ENSO that consists of both the balanced and unbalanced thermocline depth variations. The purpose of this study is to explore a stationary (nonzonally propagating) SST mode to understand the physical mechanism responsible for the phase transition of ENSO. We intend to address the following questions: What is the role of the zonal-mean thermocline depth variation in the ENSO cycle? What determines the phase lag between subsurface and surface variations? What is the effect of the basic states and the basin width on the
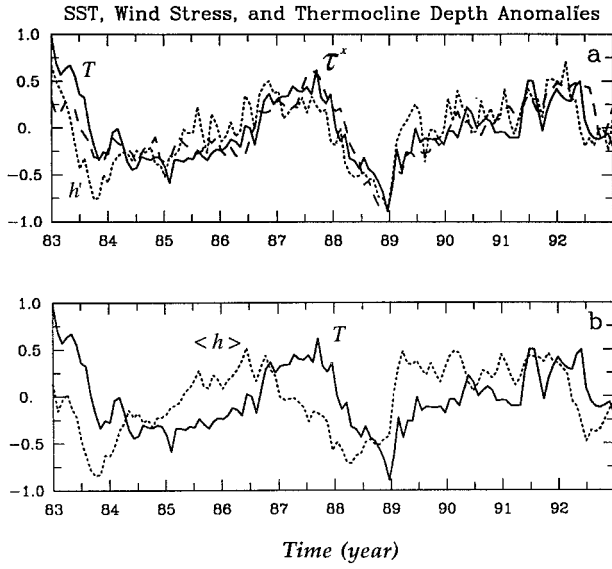
FIG. 3. (a) The time series (1983–92) of observed interannual anomalies of SST at (110°W, 0°N) (the solid line), zonal wind stress at (170°W, 0°N) (the dashed line), and the zonally asymmetric thermocline depth at (110°W, 0°N) (the dotted line). The SST, wind stress, and thermocline depth anomalies were normalized by 4.0°C, 0.5 dyn cm^{-2} and 60 m, respectively. (b) The time series of the zonal-mean thermocline depth anomaly (the dotted line) and the SST anomaly at (110°W, 0°N) (the solid line). The zonal-mean thermocline depth anomaly was normalized by 25 m.

interannual oscillation? This paper is organized as follows. In section 2, a simple dynamic model of ENSO is constructed. In section 3 we analyze the growth rates and oscillation features of the stationary SST mode and examine the sensitivity of the mode to the ocean basin width, the basic state, and the coupling strength. In section 4 we summarize our results and discuss the physical interpretation and limitation of the current model.

2. A conceptual model of the El Niño–Southern Oscillation

The dynamic framework of this conceptual model is intended to be similar to that of Zebiak and Cane (1987). The ocean component is a modified shallow water model that describes reduced-gravity upper-ocean current and thermocline variations (Cane 1979). A constant-depth mixed layer is specified in the upper ocean to describe surface temperature changes. The governing equations for mean upper-ocean current and thermocline depth anomalies, linearized by a basic state that can be either an annual-mean or a seasonal-cycle state, are written as

$$\frac{\partial u}{\partial t} - \beta y v + g\frac{\partial h}{\partial x} = \frac{\tau^x}{\rho H} - \varepsilon u, \qquad (2.1)$$

$$\beta y u + g\frac{\partial h}{\partial y} = 0, \qquad (2.2)$$

$$\frac{\partial h}{\partial t} + H\left(\frac{\partial u}{\partial x} + \frac{\partial v}{\partial y}\right) = -\varepsilon h, \qquad (2.3)$$

where u and v represent the zonal and meridional components of upper-ocean currents, h and H are anomalous and mean thermocline depth, g is the reduced gravity, ε stands for a damping coefficient, and τ^x is the zonal component of surface wind stress. In (2.1)–(2.3) we have applied the long-wave approximation and omitted the meridional wind stress component.

A derivation of $(\partial/\partial y)[\partial(2.1)/\partial y - \partial(2.2)/\partial x]$ leads to

$$\left(\frac{\partial}{\partial t} + \varepsilon\right)\left(\frac{\partial^2 u}{\partial y^2}\right) - 2\beta\frac{\partial v}{\partial y} - \beta\frac{\partial u}{\partial x} - \beta y\frac{\partial}{\partial y}\left(\frac{\partial u}{\partial x} + \frac{\partial v}{\partial y}\right)$$

$$= \frac{\partial^2}{\partial y^2}\left(\frac{\tau^x}{\rho H}\right). \qquad (2.4)$$

Substituting (2.3) to (2.4), we have

$$\left(\frac{\partial}{\partial t} + \varepsilon\right)\left(h + \frac{H}{2\beta}\frac{\partial^2 u}{\partial y^2}\right) + \frac{H}{2}\frac{\partial u}{\partial x} - \frac{Hy}{2}\frac{\partial}{\partial y}\left(\frac{\partial u}{\partial x} + \frac{\partial v}{\partial y}\right)$$

$$= \frac{1}{2\beta\rho}\frac{\partial^2 \tau^x}{\partial y^2}. \qquad (2.5)$$

Equation (2.2) may be written as

$$\frac{\partial^2 u}{\partial y^2} = -\frac{y}{3}\frac{\partial^3 u}{\partial y^3} - \frac{g}{3\beta}\frac{\partial^4 h}{\partial y^4}. \qquad (2.6)$$

Substituting (2.6) to (2.5), and setting $y = 0$ (i.e., at the equator), we have

$$\left(\frac{\partial}{\partial t} + \varepsilon\right)\left(h - \frac{gH}{6\beta^2}\frac{\partial^4 h}{\partial y^4}\right) + \frac{H}{2}\frac{\partial u}{\partial x} = \frac{1}{2\beta\rho}\frac{\partial^2 \tau^x}{\partial y^2}. \quad (2.7)$$

Along the western ($x = x_0$) and eastern ($x = x_1$) oceanic boundaries, the normal component of the current should vanish. By applying the boundary condition and integrating (2.7) zonally from x_0 to x_1, we have

$$\left(\frac{\partial}{\partial t} + \varepsilon\right)\left(\langle h\rangle - \frac{gH}{6\beta^2}\frac{\partial^4\langle h\rangle}{\partial y^4}\right) = \frac{1}{2\beta\rho}\frac{\partial^2\langle\tau^x\rangle}{\partial y^2}, \quad (2.8)$$

where $\langle S\rangle = 1/(x_1 - x_0)\int_{x_0}^{x_1} S\, dx$ denotes the zonal average within the basin and S is an arbitrary variable.

For a given low-frequency oscillating zonal wind stress that has a Hermit–Gaussian meridional structure:

$$\tau^x = \tau_0^x\left(1 - m\frac{y^2}{L_a^2}\right)\exp\left(-\frac{y^2}{2L_a^2}\right), \qquad (2.9)$$

{where $m = 2$ and $\tau_0^x = \tau_{00}^x \cos[(2\pi/80°)(x - 160°W)]$ if $160°E < x < 120°W$ and $\tau_0^x = 0$ elsewhere} with a half-width given by the atmospheric radius of deformation, $L_a = 1000$ km, the meridional structure of the zonal-mean thermocline depth anomaly can be given by

$$\langle h\rangle = \langle h\rangle|_{y=0}\left(1 + k\frac{y^2}{L_y^2} + l\frac{y^4}{L_y^4}\right)\exp\left(-\frac{y^2}{2L_y^2}\right), \quad (2.10)$$

where $k = 1.7$, $l = -0.8$, and $L_y = 850$ km. The meridional profile (2.10) was obtained based on numerical

TABLE 1. List of standard parameter values in the model.

β	$2.28 \times 10^{-11} \, \mathrm{m^{-1} s^{-1}}$	$\alpha = \rho_a C_D V_0$	$9 \times 10^{-3} \, \mathrm{kg \, m^{-2} \, s^{-1}}$
H_1	50 m	ρ_a	$1.2 \, \mathrm{kg \, m^{-3}}$
$\underline{H}$	150 m	C_D	1.5×10^{-3}
$\underline{w_1}$	$5 \times 10^{-6} \, \mathrm{m \, s^{-1}}$	V_0	$5 \, \mathrm{m \, s^{-1}}$
$\underline{T_z}$	$0.1 \, \mathrm{K \, m^{-1}}$	λ	0.25
$\overline{T_x}$	$-0.33 \times 10^{-6} \, \mathrm{K \, m^{-1}}$	$g = C_o^2/H$	$4.2 \times 10^{-2} \, \mathrm{m \, s^{-2}}$
γ	$0.1 \, \mathrm{km^{-1}}$	c_o	$2.5 \times 10^{-2} \, \mathrm{m \, s^{-1}}$
ε_a	$(2 \, \mathrm{day})^{-1}$	L_x	$8 \times 10^6 \, \mathrm{m}$
r_s	$(2 \, \mathrm{day})^{-1}$	L_a	$10^6 \, \mathrm{m}$
ε	$(2 \, \mathrm{year})^{-1}$	L_y	$8.5 \times 10^5 \, \mathrm{m}$
μ	$(2 \, \mathrm{year})^{-1}$	A	$51 \, \mathrm{m^2 \, s^{-2} \, K^{-1}}$
Π	0.42	Θ	$1.75 \times 10^{-8} \, \mathrm{s^{-1}}$
Ω	$1.0 \times 10^{-8} \, \mathrm{K^{-1} s^{-1}}$	Λ	$2.38 \times 10^{-7} \, \mathrm{m \, K^{-1} \, s^{-1}}$

FIG. 4. The meridional structure of the zonal wind stress anomaly (the solid line) and the zonal-mean thermocline depth anomaly (the dotted line).

integration of the shallow water model (2.1)–(2.3) in a rectangle Pacific basin (120°E–80°W and 40°S–40°N). In this calculation the prescribed wind stress forcing has a 3-yr oscillation period. All parameters have standard values listed in Table 1. The parameters k, l, and L_y were determined using the least-squares method by projecting the numerical solution into a series of Hermit-Gaussian functions. The projected profile is very close to the original solution. Figure 4 shows the two meridional profiles.

Equation (2.8) can therefore be further simplified as

$$\left(\frac{\partial}{\partial t} + \varepsilon \right) \langle h \rangle = - \frac{(2m + 1)}{2\beta\rho(1 + n)L_a^2} \langle \tau^x \rangle, \quad (2.11)$$

where $n = gH(4k - 8l - 1)/2\beta^2 L_y^4 = 0.14$ is a structure parameter representing the meridional profile of the zonal-mean thermocline depth anomaly. The negative sign for the rhs of (2.11) states that a positive $\langle \tau^x \rangle$ at the equator or a negative $\langle \tau^x \rangle$ off the equator—a typical case during El Niño—leads to a negative tendency for $\langle h \rangle$. Physically, the two following processes may contribute to such a negative tendency: 1) Rossby waves are efficiently generated in regions of wind curl, and the passage and reflection of these waves throughout the basin may cause the delayed response of the zonal-mean thermocline depth anomaly at the equator; 2) the zonal-mean mass transport is induced by intensified off-equatorial winds through the zonal-mean divergence of meridional currents in the upper ocean.

The specification of the meridional structure of zonal wind stress in (2.9) is based on the 10-yr (1983–92) observational dataset. Figure 5a illustrates that the zonal-mean zonal wind stress off the equator (at 10°N) has an opposite sign as that at the equator. Using different datasets, Nigam and Shen (1993) and Oort and Yienger (1996) showed that the interannual anomaly of surface and upper-troposphere zonal winds at the equator is in general out of the phase with that in the extratropics (Fig. 6a). This is physically understandable since a warm episode in the eastern equatorial Pacific, on one hand, causes the intensification of a reversed Walker circulation and therefore westerly wind anomalies at the equator, and, on the other hand, leads to the strength-
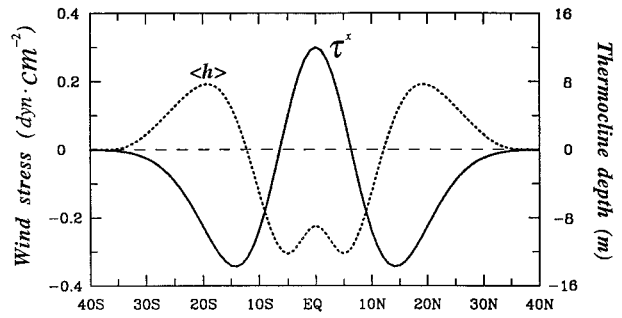
ening of the local Hadley cell, through anomalous heating source over the central equatorial Pacific, that further intensifies the subtropical highs and thus easterly trades off the equator. The close association between subtropical pressure anomalies and the El Niño was documented from an observational analysis by Wang (1995), who found that during 1950–92 the surface pressure anomalies at the northwestern (10°–25°N, 130°–175°E) and southwestern Pacific (15°–30°S, 160°E–170°W) is highly correlated with equatorial SST anomalies (Fig. 6b).

To examine the sensitivity of equatorial thermocline response to the meridional wind structure, we conduct the two following experiments using the shallow water model (2.1)–(2.3). In the first experiment (a reference case), a Hermit-Gaussian profile ($m = 2$) is used, and in the second, a Gaussian profile ($m = 0$) is specified. In both cases the forcing has a 3-yr oscillation period.
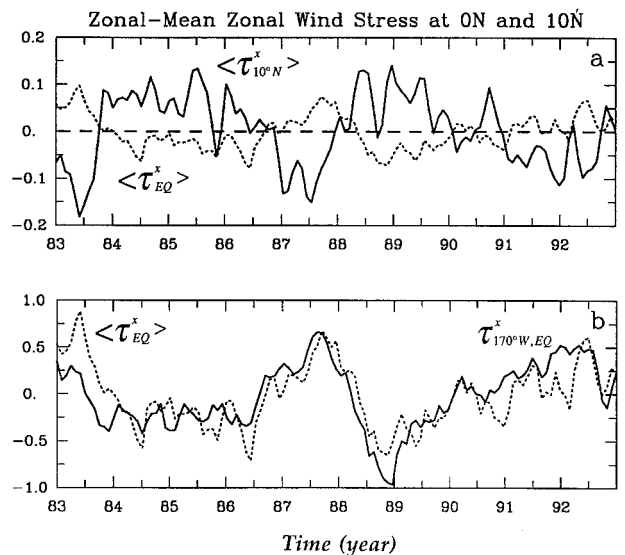

FIG. 5. (a) The time series (1983–92) of observed zonal-mean zonal wind stress anomalies at the equator (the dotted line) and at 10°N (the solid line). (b) The time series of the maximum zonal wind stress anomaly at (170°W, 0°N) (the solid line) and the zonal-mean equatorial zonal wind stress anomaly (the dotted line). The wind stresses in (b) were normalized by 0.5 and 0.1 dyn cm^{-2}, respectively.
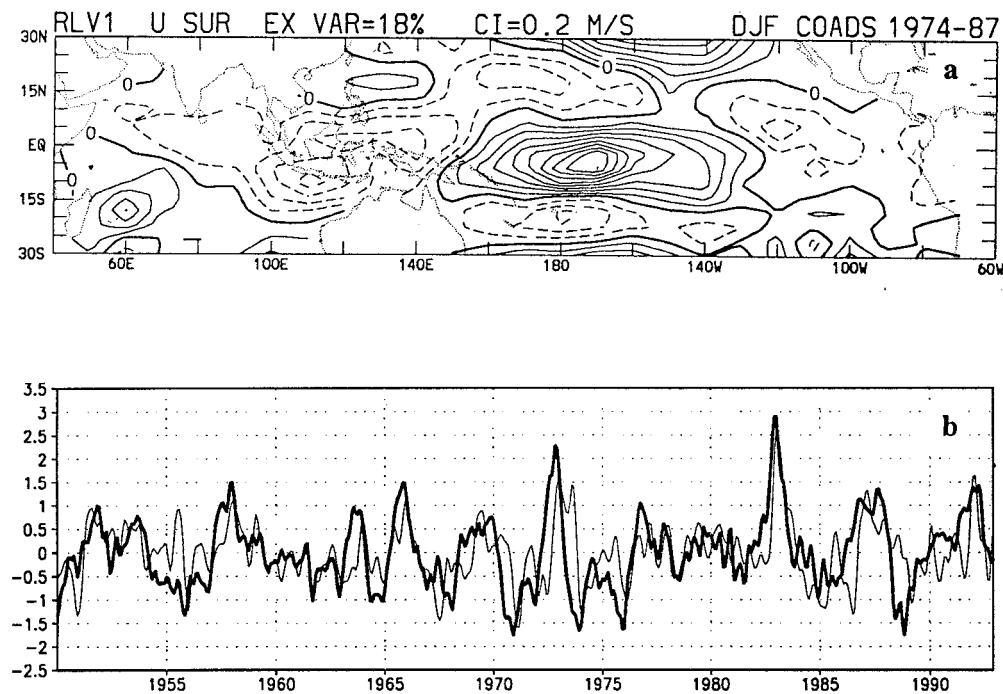
FIG. 6. (a) The structure of the leading mode of surface zonal wind component (interval: 0.2 m s^{-1}) during the 1974–87 winter seasons [adopted from Nigam and Shen (1993)]. (b) The time series (1950–92) of the SST anomaly (in °C, the solid line) in the equatorial Pacific (5°S–5°N, 155°–110°W) and the SLP anomalies (in mb, the dotted line) at the northwestern Pacific (130°–175°E, 10°–25°N) (derived from Wang 1995).

(Our sensitivity tests using different forcing periods (2 and 4 yr, respectively) indicate that the phase lag between $\langle h \rangle$ and τ^x is relatively insensitive.) Figure 7a illustrates the time evolution of $\langle h \rangle$ in the two cases (the solid line denotes $m = 2$ case and the dashed line denotes $m = 0$ case). To compare with observations, a calculation based on the time series of Fig. 3b, using an optimum lagged correlation method, is conducted and the result indicates that $\langle h \rangle$ leads τ^x (or SST) for approximately 8 months. It is noted that the Hermit-Gaussian wind distribution results in a more realistic phase lag. To test whether such a phase lag is sensitive to the friction coefficient, two sensitivity experiments are conducted in which ε is either reduced by half or doubled. The results indicate that the phase lag is not sensitive to ε (figure not shown).

The role of off-equatorial winds on the $\langle h \rangle - \tau^x$ phase lag is further revealed by designing a parallel experiment in which only the winds off the equator are presented (the winds between 7°S and 7°N are artificially set to be zero). [The same wind profile as (2.9) is applied in that case.] The results, as shown in the dotted line of Fig. 7a, indicate that 1) in the absence of equatorial wind forcing, the off-equatorial wind stress itself can generate a delayed response of $\langle h \rangle$ at the equator; 2) to a large extent, the phase difference between $\langle h \rangle$ and τ^x is controlled by off-equatorial wind processes (note that the phase lags in both the off-equatorial-wind-only case and the reference case are almost identical). This implies

a new possible mechanism for ENSO transition—an enhanced local Hadley cell changes subtropical pressures and thus off-equatorial winds that further alter the thermocline at the equator.

One important issue regarding the phase lag between $\langle h \rangle$ and τ^x (or $\langle \tau^x \rangle$, since $\langle \tau^x \rangle$ and τ^x are approximately in phase, see Fig. 5b) is what is the role of oceanic waves and their reflection at the coast. As indicated by Philander et al. (1992), a host of oceanic waves can be excited by periodic winds. If the period of the winds were on the order of a few weeks, then only equatorial Kelvin waves would be excited (Philander and Pacanowski 1981). With the increase of the forcing period more and more Rossby waves come into play, so that the pattern of phase propagation becomes very complex, and it is no longer possible to identify an individual oceanic (Kelvin or Rossby) wave. It follows that on the interannual timescales, the response of the ocean to the winds should be considered as a result of accumulated effects of various (including coastal-reflected) waves. To identify the role of these waves and their reflection at the coast, we design an experiment, parallel to the reference case, in which the western boundary of the ocean is extended 160° longitudes toward the west, with strong damping applied in the new western boundary to prevent possible wave reflections. The purpose of this experiment is to examine how the zonal-mean equatorial thermocline responds in the absence of (reflected) waves. The same forcing (as in the reference case) is
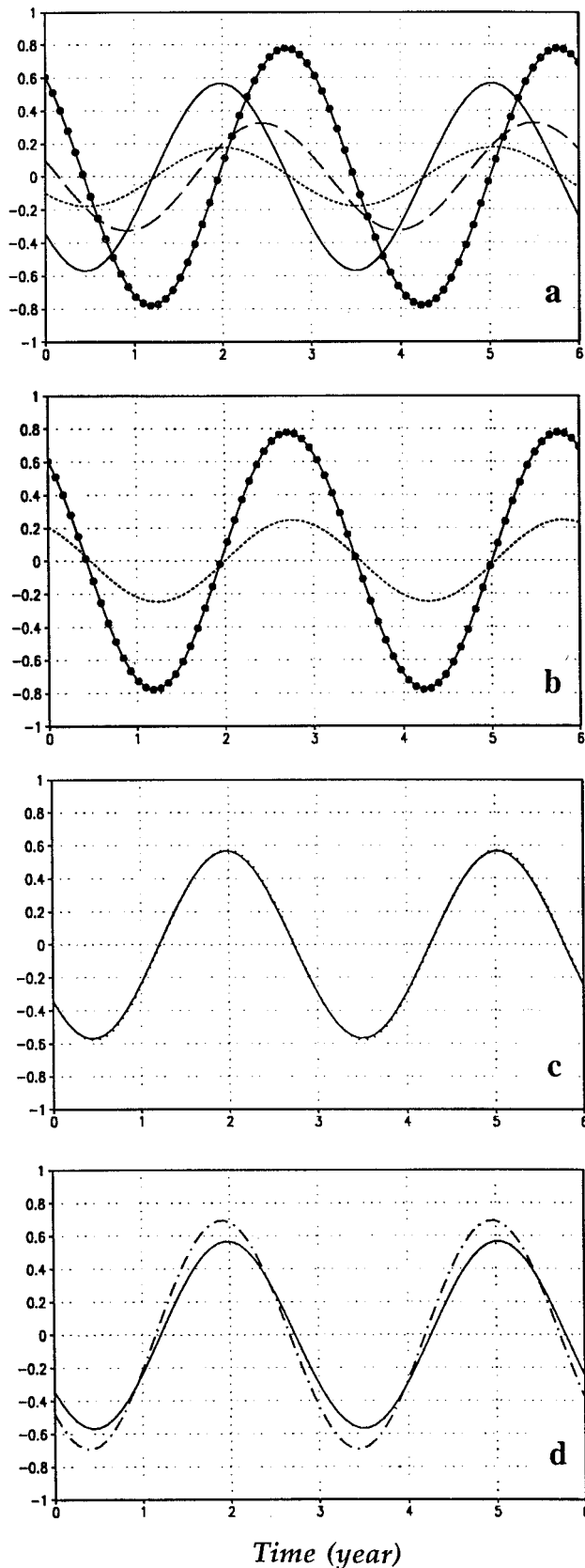
applied. The dotted line in Fig. 7b shows the response of $\langle h \rangle$ in this case. Note that there is no phase lag between $\langle h \rangle$ and τ^x. On the other word, they are approximately in equilibrium. The experiment clearly demonstrates the importance of the ocean waves and their reflection in the western boundary in determining the phase lag.

Another issue is whether or not the meridional component of wind stress is critical in the phase transition of ENSO. It is possible that this component of wind stress may cause a coupled instability by inducing upwelling or downwelling through the surface divergence of meridional currents. It is not clear, however, whether it can cause a phase transition. To examine this question, we conduct two additional experiments, using an unapproximated (no long-wave approximation) shallow water model in which the meridional component of wind stress is specified as

$$\tau^y = \tau_0^y \frac{y}{L_a} \exp\left(-\frac{y^2}{2L_a^2}\right), \qquad (2.12)$$

where $\tau_0^y = \tau_{00}^y \cos[(2\pi/80°)(x - 120°\text{W})]$ if $160°\text{W} < x < 80°\text{W}$ and $\tau_0^y = 0$ elsewhere; and $\tau_{00}^y = -\tau_{00}^y$. The corresponding meridional wind has a maximum convergence (divergence) of 4×10^{-6} s^{-1} at the equator. Figure 7c shows that this component of wind stress has little effect on the $\langle h \rangle - \tau^x$ phase lag relationship.

Equation (2.11) states that the zonal-mean thermocline depth anomaly at the equator is *not* in equilibrium with the zonal wind stress anomaly. A positive zonal wind stress (or SST) anomaly leads to a negative time tendency for $\langle h \rangle$. This agrees well with the observations (Fig. 3b) and with oceanic GCM experiments (Schneider et al. 1995).

It is worth noting that the only approximation made in deriving (2.11) from (2.1)–(2.3) is the specification of the meridional structure of τ^x and $\langle h \rangle$ [Eqs. (2.9) and (2.10)]. To validate the approximation, it is necessary to compare the solution calculated directly from (2.11) with that from (2.1)–(2.3) (the reference case). Figure 7d shows that they are quite close.

For the special case of $\varepsilon = 0$, $\langle h \rangle$ and $\langle \tau^x \rangle$ have exactly a 90° phase lag, implying that a maximum (zero) wind anomaly corresponds to a zero (maximum) phase in $\langle h \rangle$.

Time (year)

FIG. 7. (a) The time evolution of the zonal-mean thermocline depth anomaly at the equator in the presence of the Hermit-Gaussian wind distribution [the solid line in (a), (c), and (d)], the Gaussian wind distribution (the dashed line), and the off-equatorial wind only (the dotted line). (b) The time evolution of $\langle h \rangle$ (the dotted line) in the case when the western boundary of the ocean is extended 160° toward the west. The solid circle lines in both (a) and (b) denote the time evolution of zonal wind stress at the equator. (c) The time evolution of $\langle h \rangle$ (the dotted line) in the case when the meridional wind stress is included. (d) The time evolution of $\langle h \rangle$ (the dot–dashed line) calculated from (2.11). In all four panels $\langle h \rangle$ and τ^x have been normalized by 15 m and 0.4 dyn cm^{-2}, respectively.

In general, the phase lag varies around the special value, depending on the ratio of the reversed Newtonian damping timescale and the period of oscillation. The phase lag relationship is of practical use for ENSO forecasts. For instance, during a transition phase of ENSO, while surface conditions are normal, subsurface temperatures are substantially abnormal. In that case the crucial factor lies in the initial condition of the subsurface ocean.

A single equation for h at the equator is readily derived from (2.1)–(2.3), which is

$$\left(\frac{\partial}{\partial t} + \varepsilon\right)\left(\frac{2}{y}\frac{\partial h}{\partial y} - \frac{\partial^2 h}{\partial y^2}\right) - \beta\frac{\partial h}{\partial x} = -\frac{\beta\tau^x}{\rho g H}. \quad (2.13)$$

Consider a scale analysis for (2.13). Taking a half-width of the basin $L/2$, a quarter of interannual oscillation period $\tau/4$, and the mean mixed-layer depth H_1 as characteristic zonal length, time, and thermocline displacement scales, and setting $L = 160°$ and $\tau = 3$ years, we have

$$\frac{O\left[\left(\dfrac{\partial}{\partial t} + \varepsilon\right)\left(\dfrac{2}{y}\dfrac{\partial h}{\partial y} - \dfrac{\partial^2 h}{\partial y^2}\right)\right]}{O\left(\beta\dfrac{\partial h}{\partial x}\right)} = \frac{4L_x(2k-1)}{\beta\tau L_y^2} \approx 0.05 \ll 1.$$

$$(2.14)$$

In (2.14) we have assumed that h has the same meridional structure as (2.10). In the lowest order of approximation (2.13) can be simplified as

$$\frac{\partial h}{\partial x} = \frac{\tau^x}{g\rho H}, \quad (2.15a)$$

or

$$\frac{\partial h'}{\partial x} = \frac{\tau^x}{g\rho H}, \quad (2.15b)$$

where $h' = h - \langle h \rangle$ denotes the zonally asymmetric thermocline depth anomaly.

Using a different approach, Neelin (1991) derived the same equation as (2.15). The difference is that he did not consider the nonequilibrium of the zonal-mean thermocline depth anomaly, rather he only considered the zonally asymmetric part that is in the Sverdrup balance with the wind. We shall demonstrate that in this model it is the nonequilibrium of the zonal-mean thermocline depth anomaly that is crucial for the phase transition of ENSO.

Following Zebiak and Cane (1987), the surface currents and the vertical entrainment velocity at the base of the mixed layer are determined by a sum of the mean upper-ocean component and the Ekman shearing component:

$$u_1 = u + \frac{H_2}{H}u_s = -\frac{g}{\beta y}\frac{\partial h}{\partial y} + \frac{H_2}{H}u_s, \quad (2.16)$$

$$w_1 = w + \frac{H_2}{H}w_s = -\frac{H_1}{H}\left(\frac{\partial}{\partial t} + \varepsilon\right)h$$

$$+ \frac{H_1 H_2}{H}\left(\frac{\partial u_s}{\partial x} + \frac{\partial v_s}{\partial y}\right), \quad (2.17)$$

where $H_2 = H - H_1$. The shearing currents between the mixed layer and the layer below are governed by

$$r_s u_s - \beta y v_s = \frac{\tau^x}{\rho H_1}, \quad (2.18)$$

$$r_s v_s + \beta y u_s = 0. \quad (2.19)$$

The atmospheric component of the coupled model is based on a simplified Lindzen and Nigam (1987) model in which the surface winds, (u_a, v_a), are determined by SST-gradient induced pressure gradients:

$$\varepsilon_a u_a - \beta y v_a = A\frac{\partial T}{\partial x}, \quad (2.20)$$

$$\varepsilon_a v_a + \beta y u_a = A\frac{\partial T}{\partial y}, \quad (2.21)$$

where ε_a is the Rayleigh friction coefficient and $A = 9.8H_0/2T_0$ is a coefficient reflecting the strength of boundary-layer pressure gradients induced by SST gradients ($H_0 = 3000$ m and $T_0 = 288$ K). At the equator, the zonal wind stress can be written as

$$\tau^x = \alpha u_a = \frac{\alpha A}{\varepsilon_a}\frac{\partial T}{\partial x}, \quad (2.22)$$

where $\alpha = \rho_a C_D V_0$. Note that the above phase relationship between τ^x and T is generally in agreement with the leading EOF mode structure (Fig. 2).

Linearized about a basic state that can be either the climatological annual-mean or seasonal-cycle state, the time dependence of the SST anomaly at the equator can be expressed as

$$\frac{\partial T}{\partial t} = -u_1\overline{T}_x - \overline{u}_1 T_x - w_1\overline{T}_z - \frac{\overline{w}_1}{H_1}(T - \gamma h) - \mu T,$$

$$(2.23)$$

where $\overline{T}_x$, $\overline{T}_z$, $\overline{u}_1$, and $\overline{w}_1$ represent the basic-state zonal and vertical temperature gradient, surface zonal current, and vertical entrainment velocity at the base of the mixed layer, respectively; γ is a parameter that controls the changes in subsurface temperatures due to the thermocline displacement; and μ is a thermal dissipation coefficient. In (2.23) we have neglected anomalous meridional temperature advection, assuming that interannual oscillations are strictly symmetric about the equator.

The principal simplification of the current model derives from the fact that the interannual SST mode is

essentially a stationary oscillation mode. Therefore in a zero order of approximation, the SST and zonal wind anomalies can be assumed to have a fixed zonal structure (as in Fig. 2). The specification of the longitudinal profiles of the SST and wind fields helps to filter out the zonally propagating SST mode (discussed by Neelin 1991) and allows us to focus on discussing a new, so-called stationary SST mode. Let us consider the time evolution of the SST at a particular location, say 110°W at the equator, where the interannual SST anomaly has a maximum. Assume $T(x, t) = T_E(t)f_1(x)$ and $\tau^x(x, t) = \tau_C^x(t)f_2(x)$, where $f_1(x)$ and $f_2(x)$ are the longitudinal functions as shown in Fig. 2, and T_E and τ_C^x are amplitudes, representing maximum temperature and wind stress in the eastern (denoted by subscript E) and central (denoted by subscript C) Pacific, respectively. From (2.22), (2.15b), (2.16), and (2.17), we have

$$\tau_c^x = \frac{\alpha A}{\varepsilon_a L_x} T_E, \tag{2.24}$$

$$h'_E = \frac{\alpha A}{\rho g H \varepsilon_a} T_E, \tag{2.25}$$

$$u_{1E} = -\frac{g(2k-1)}{\beta L_y^2}(\langle h \rangle + h'_E), \tag{2.26}$$

$$w_{1E} = -\frac{H_1}{H}\left(\frac{\partial}{\partial t} + \varepsilon\right)(\langle h \rangle + h'_E) - \frac{H_2}{\rho H r_s L_x}\tau_c^x. \tag{2.27}$$

Set $\langle \tau^x \rangle = \lambda \tau_c^x$, thus the time dependence of T_E abides by

$$\frac{dT_E}{dt} = \left(\frac{\overline{T}_z H_2 \alpha A}{\rho H r_s \varepsilon_a L_y^2} - \frac{\overline{w}_1}{H_1} - \mu\right)T_E$$

$$+ \left[\frac{\overline{w}_1 \gamma}{H_1} + \frac{\overline{T}_x g(2k-1)}{\beta L_y^2}\right]h_E + \frac{\overline{T}_z H_1}{H}\left(\frac{d}{dt} + \varepsilon\right)h_E. \tag{2.28}$$

Given the standard parameter values listed in Table 1, we have

$$\frac{\overline{T}_x g(2k-1)}{\beta L_y^2} \ll \frac{\overline{w}_1 \gamma}{H_1}, \tag{2.29}$$

and

$$\frac{\overline{T}_z H_1}{H}\varepsilon \ll \frac{\overline{w}_1 \gamma}{H_1}. \tag{2.30}$$

Therefore, (2.28) can be further simplified as

$$(1 - \Pi)\frac{dT_E}{dt} = \Theta T_E + \Omega\langle h \rangle, \tag{2.31}$$

where

$$\Pi = \frac{\overline{T}_z H_1 \alpha A}{\rho g H^2 \varepsilon_a}, \tag{2.32}$$

$$\Theta = \frac{\overline{T}_z H_2 \alpha A}{\rho H r_s \varepsilon_a L_x^2} + \frac{\overline{w}_1 \gamma \alpha A}{H_1 \rho g H \varepsilon_a} - \frac{\overline{w}_1}{H_1} - \mu$$

$$- \frac{(2m+1)\overline{T}_z H_1 \lambda \alpha A}{2\beta\rho(1+n)L_a^2 H \varepsilon_a L_x}, \tag{2.33}$$

$$\Omega = \frac{\overline{w}_1 \gamma}{H_1}. \tag{2.34}$$

The zonal-mean thermocline depth equation (2.11) may be rewritten as

$$\frac{d\langle h \rangle}{dt} = -\Lambda T_E - \varepsilon\langle h \rangle, \tag{2.35}$$

where $\Lambda = [(2m+1)\lambda\alpha A]/[2\beta\rho(1+n)L_a^2\varepsilon_a L_x]$. Table 1 lists the standard values for Π, Θ, Ω, and Λ.

Equations (2.31) and (2.35) form a simplest, linear ENSO dynamic system. Within this system two important feedback processes are worth noting. The first one involves a positive feedback between the surface wind, SST, and the zonally asymmetric part of the thermocline depth anomalies, as seen from the first two terms on the right-hand side of (2.33)—the first term represents anomalous upwelling by mean stratification and the second term reflects the effect of subsurface temperature variations. The second one involves a negative feedback between the zonal-mean thermocline depth anomaly and the wind (or SST) anomaly, as depicted from the term Λ—a positive SST anomaly in the eastern Pacific leads to a negative tendency for the zonal-mean thermocline depth anomaly which, in turn, decreases SST and eventually brings a cold episode. Both types of feedback processes are crucial for ENSO in the sense that whereas the positive feedback tends to overcome dissipation and maintain an interannual anomaly, the negative feedback is responsible for the phase transition. When $\Lambda = 0$, $\langle h \rangle$ and SST are decoupled. In that case there is no interannual oscillation.

3. Analyses of the stationary SST mode

For given an annual mean basic state, the linear ENSO dynamic system (2.31) and (2.35) can be further derived into a constant-coefficient, second-order differential equation:

$$\frac{d^2T_E}{dt^2} + \left(\varepsilon - \frac{\Theta}{1-\Pi}\right)\frac{dT_E}{dt} + \frac{\Lambda\Omega - \varepsilon\Theta}{1-\Pi}T_E = 0. \tag{3.1}$$

The growth rate and frequency of the stationary SST mode are

$$\omega_r = \frac{1}{2}\left(\frac{\Theta}{1-\Pi} - \varepsilon\right), \tag{3.2}$$

$$\omega_i = \frac{1}{2}\sqrt{\Delta}; \tag{3.3}$$

Growth Rate (1/year)

Growth Rate (1/year)

Oscillation Period (year)

Oscillation Period (year)
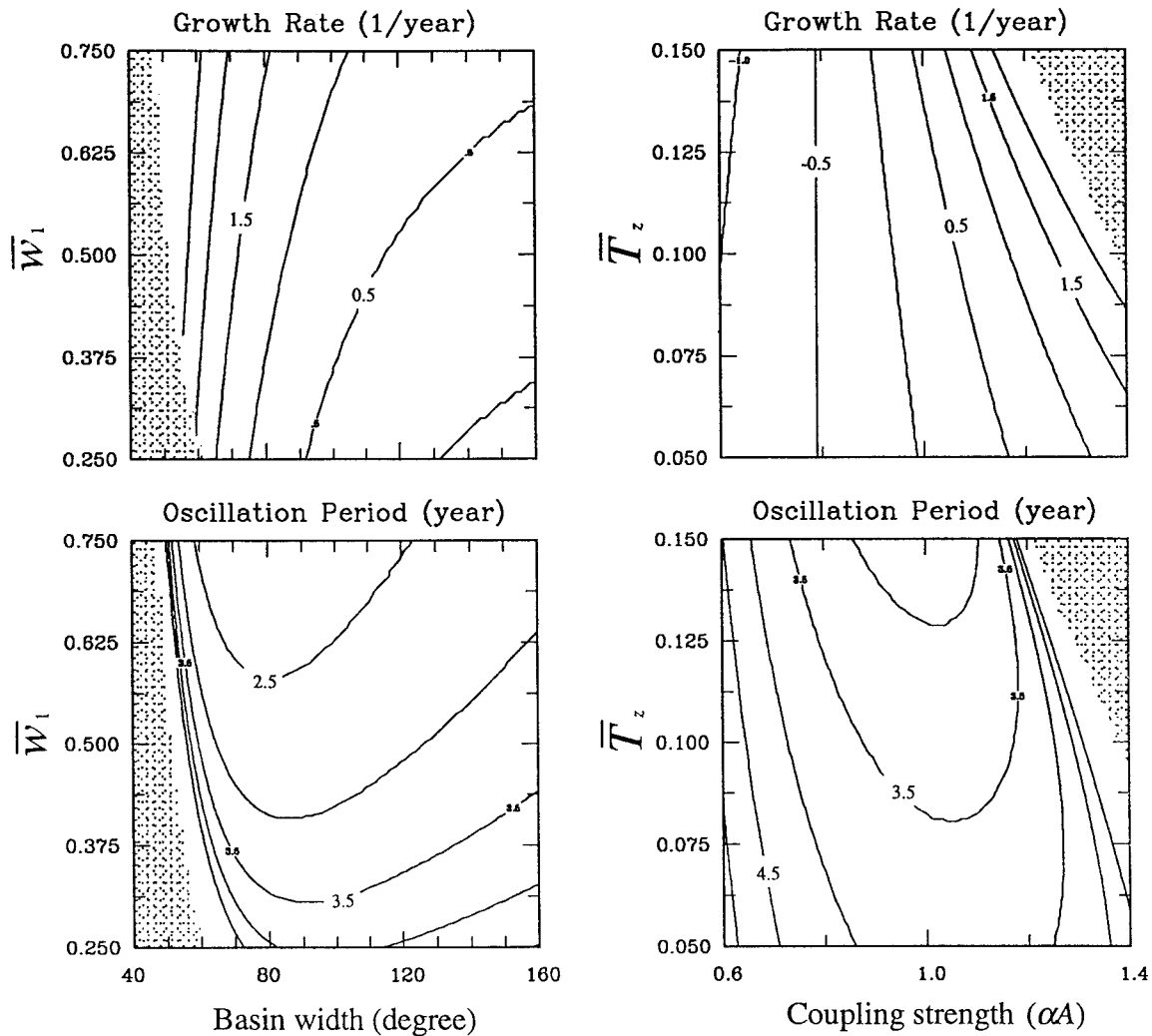
Basin width (degree)

Coupling strength (αA)

FIG. 8. The growth rate and oscillation period of the stationary SST mode as a function of the ocean basin width and the basic-state vertical velocity at the base of the mixed layer (the left panels) and as a function of air–sea coupling strength and the basic-state upper-ocean stratification (the right panels). Shaded regions denote no oscillation solutions.

and the necessary and sufficient condition for obtaining an oscillative solution is

$$\Delta = \frac{4(\Lambda\Omega - \varepsilon\Theta)}{(1 - \Pi)} - \left(\frac{\Theta}{1 - \Pi} - \varepsilon\right)^2 > 0. \quad (3.4)$$

a. Dependence on the basin width, basic state, and coupling strength

For the standard parameter values listed in Table 1, the model has an interannual oscillation solution, with a period of 40 months and a growth rate of 0.25 yr^{-1} (which corresponds to an e-folding timescale of 4 yr). Figure 8 shows that the growth rates and oscillation periods depend on the width of the ocean basin, on the basic-state vertical motion and temperature gradient, and on air–sea coupling strength.

It is interesting to note that the stationary SST mode is basin dependent. No oscillation solutions can be found when the basin width is less than 50° in longitude, suggesting that ENSO-like interannual variability in the equatorial Atlantic may result from different mechanisms. In fact, a recent observational study by Nobre and Shukla (1996, personal communication) showed that the dominant mode of interannual SST and wind variations in the tropical Atlantic is asymmetric about the equator. The growth rate is also influenced by the basin width. The larger the dimension of the basin, the smaller the coupled instability.

The basic-state vertical motion and stratification and air–sea coupling strength are other factors that control the instability and frequency of the stationary SST mode. The larger the basic-state upwelling and the stronger the upper-ocean stratification, the greater the growth rate, and the shorter the oscillation period. Too strong
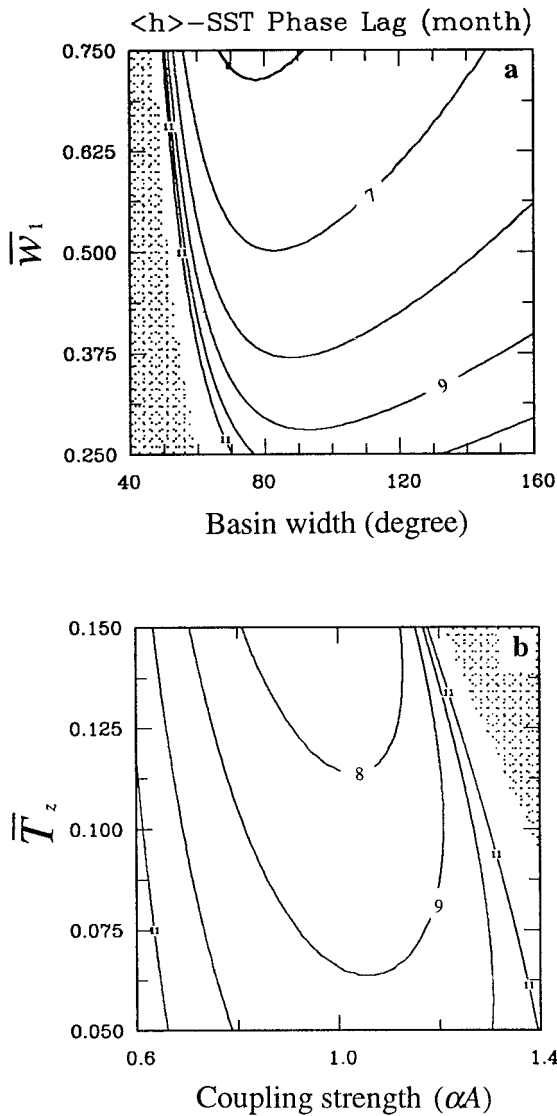
FIG. 9. Phase lags (units: month) between $\langle h \rangle$ and SST as a function of (a) the width of the ocean basin and the basic-state vertical motion and (b) the air–sea coupling strength and the basic-state stratification.

or too weak coupling leads to no interannual oscillations.

b. Phase lag between $\langle h \rangle$ and SST

The interannual oscillation in the stationary SST mode results from the delayed response of the zonal-mean thermocline depth anomaly to the wind forcing. From (2.35) one can readily derive the phase lag angle between $\langle h \rangle$ and T_E (or τ^x):

$$\delta = \tan^{-1} \frac{\omega_i}{\omega_r + \varepsilon}, \qquad (3.5)$$

where δ represents the $\langle h \rangle - \tau^x$ phase lag angle. A positive value of δ implies that $\langle h \rangle$ leads τ^x. For the
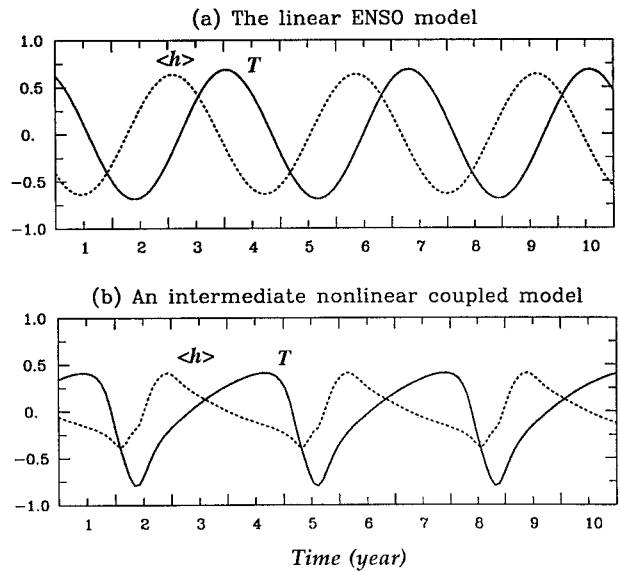

FIG. 10. The time evolution of the zonal-mean thermocline depth anomaly and the SST anomaly in the eastern equatorial Pacific calculated from (a) our linear dynamic model and (b) an intermediate Cane–Zebiak type model. The amplitudes of $\langle h \rangle$ and SST were normalized by 25 m and 4°C, respectively.

parameter values in Table 1, $\delta = 75°$, corresponding to a phase delay of 8 months. Figure 9 illustrates that the phase lag depends on a number of factors, such as the basic state and coupling strength. For a reasonable parameter regime, it varies from 6 months to a year or so.

To compare with the above analytical solution, a 100-yr time integration of the linear dynamic system, (2.31) and (2.35), is conducted. The result shows that the zonal-mean thermocline depth anomaly indeed leads the SST anomaly. Figure 10a shows a 10-yr period of this integration. (In this calculation all parameters have the same values as in Table 1 except that the thermal damping coefficient, μ, is set to be 1/450 days. The reason for choosing such a value for μ is to obtain a neutral rather than growing oscillation.) To make sure such a phase lag relationship is not model-dependent, we performed an additional experiment (100-yr integration) using an intermediate nonlinear coupled model of Chang et al. (1995), a model that has the same dynamics as those of Zebiak and Cane (1987) except that it predicts both the seasonal and interannual variations. The results, as shown in Fig. 10b, agree well with our linear model. The phase relationship is further confirmed by the NCEP 4D data assimilation set (Fig. 3b).

c. The zonal propagation of thermocline depth anomaly at the equator

In spite of the stationary oscillation feature in the SST and wind fields, the thermocline depth anomaly exhibits clear eastward "propagation" along the equator. Figure 11 illustrates the longitude–time section of

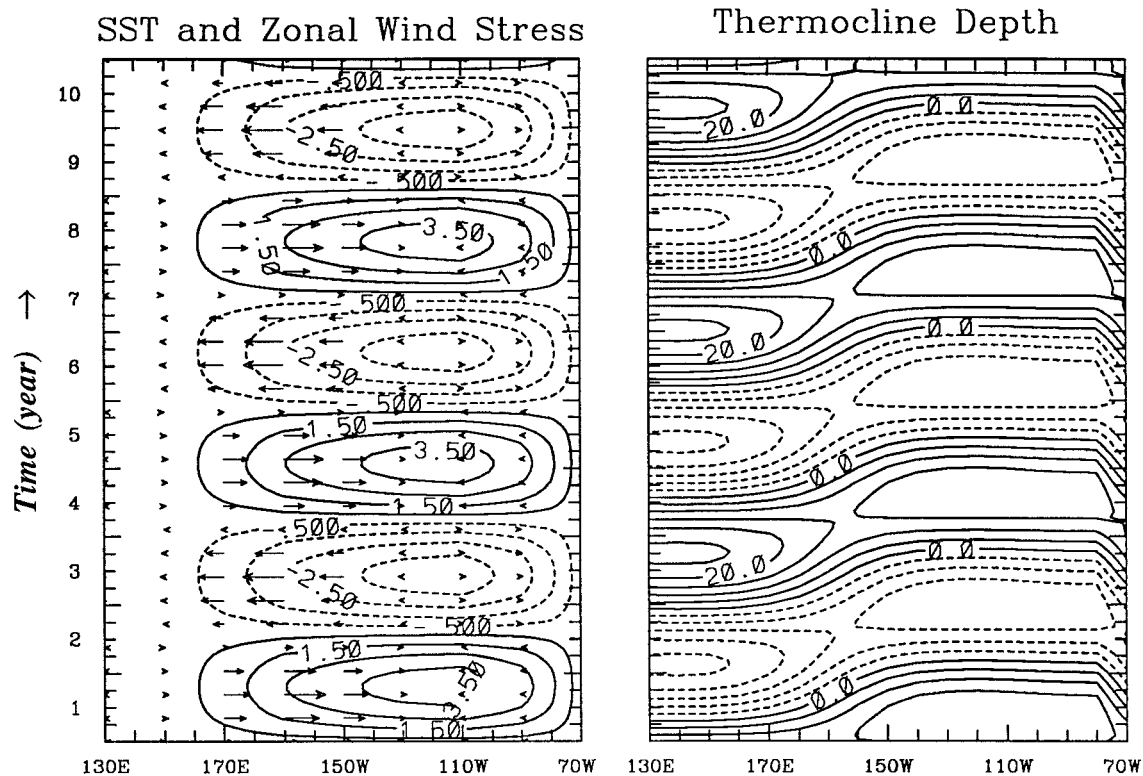## SST and Zonal Wind Stress   ## Thermocline Depth

FIG. 11. The time–longitude plots of simulated SST, zonal wind stress, and thermocline depth (including both the zonally averaged and asymmetric parts) anomalies along the equator. The contour intervals for the thermocline depth and SST anomalies are 5 m and 1°C, respectively. The maximum vector for the wind stress is 0.4 dyn cm^{-2}.

model SST, zonal wind stress, and thermocline depth anomalies at the equator. The results are derived from the above 100-yr time integration, with the specified zonal SST and wind structures (Fig. 2). The longitudinal tilt of the zonally asymmetric thermocline depth anomaly is obtained based on the Sverdrup balance (2.15b). It is the combination of both the zonal-mean and zonally asymmetric thermocline depth anomalies that causes the eastward propagation. The propagation is not a result of free ocean Kelvin waves (in fact their speeds are totally different), but a result of two different types of response of thermocline to the winds. Such a feature agrees well with observations and with coupled model simulations (e.g., Battisti and Hirst 1989; Philander et al. 1992).

d. Seasonal dependence

One important feature of ENSO is its phase locking into the seasonal cycle (Rasmusson and Carpenter 1982). A 100-yr record of interannual SST anomalies (figure omitted) indicates that the maximum anomalies in the eastern equatorial Pacific often occur late in the year, say, in December. A similar feature is the rapid drop of lagged correlation of the Southern Oscillation index during the boreal spring (Webster and Yang 1992).

To examine the seasonal dependence of the stationary

SST mode, we introduce an idealized seasonal-cycle basic state in which the vertical motion at the base of the mixed layer and the mean vertical temperature gradient in the upper ocean are

$$\overline{w}_1 = 0.5 \times 10^{-5} - 0.25 \times 10^{-5} \sin\left(\frac{2\pi i}{12}\right), \quad (3.6)$$

$$\overline{T}_z = 0.1 + 0.05 \sin\left(\frac{2\pi i}{12}\right), \quad (3.7)$$

where $i = 1, 2, \ldots, 12$, indicating January, February, . . . , December, respectively. The amplitude and phase of this seasonal cycle are determined based on coupled model simulations by Li and Philander (1996), who studied the mechanisms associated with the annual cycle at the equator. This annual cycle has stronger (weaker) upwelling and less (more) stable stratification in the northern fall (spring).

Figure 12 shows that the stationary SST mode tends to destabilize later in the year (from June through December) and stabilize earlier in the year. Note that a maximum growth rate occurs in September and a weakest and negative growth rate appears in March. The negative growth rate in March–April suggests that the basic state is not favorable for the growth of interannual oscillations during that time. This may explain why
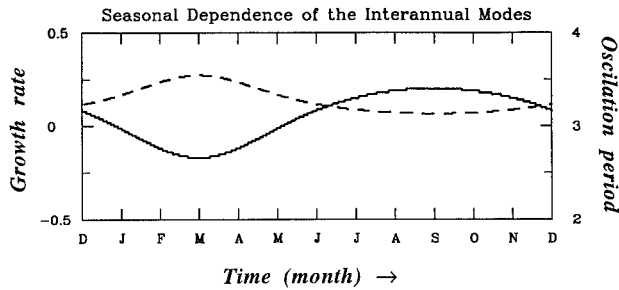
FIG. 12. The seasonal dependence of the growth rate (units: year^{-1}) (the solid line) and the oscillation period (units: year) (the dashed line) of the stationary SST mode.

there is a spring barrier in both observed and modeled Southern Oscillation signals. The persistence of positive growth rates from June through December make it possible that the mature phase of the El Niño may appear in December. This explains why maximum SST anomalies are often observed at that time.

4. Summary and discussion

Studies of the El Niño–Southern Oscillation indicate that the interactions between the ocean and atmosphere support at least two types of modes. In the first type of modes, sea surface temperature and surface wind variations can be in phase but other ocean quantities, such as the thermocline depth anomaly, have a phase lag that represents the memory of the ocean of previous winds to which it is still adjusting. The ocean waves and their reflection at coasts are important because they affect the adjustment. A typical example is the delayed oscillator mode. In the second type of modes, ocean waves and coastal reflection are of secondary importance, and the dynamic response of the ocean to the winds is an equilibrium one. That is to say that the SST, wind, and thermocline depth anomalies are always in phase with time. The timescale of the oscillation is controlled by the zonal propagation of SST. A typical example is the slow SST mode.

In this paper a stationary SST mode mechanism is proposed. This stationary SST mode essentially belongs to the first category of the coupled modes, based on the argument that the memory of the ocean lies in the subsurface ocean dynamics. It differs from the delayed oscillator mode in the sense that the current mode does not emphasize detailed wave propagation processes, rather emphasizes the accumulated effects of ocean wave dynamics on the nonequilibrium of zonal-mean thermocline adjustment. It differs from the slow SST mode in that it considers both balanced and unbalanced thermocline depth variations and does not take into account the zonal propagation of SST at the equator.

The key to the interannual oscillation in the stationary SST mode arises from the time evolution of the zonal-mean thermocline depth anomaly that is *not* in equilibrium with the winds. Because of the nonequilibrium,

this part of the thermocline depth variation tends to have a phase lag with the SST (or winds) and therefore holds a key for the phase transition of ENSO. Such a phase relationship agrees well with the NCEP 4D data assimilation (Fig. 3b) and with GCM simulations (e.g., Schneider et al. 1995).

While the zonal-mean thermocline depth anomaly is not in equilibrium with the winds, the zonally asymmetric part of the thermocline depth anomaly is in equilibrium. Based on scale analyses, we derived Eq. (2.15), the same equation as that of Neelin (1991), which states that at the equator the zonally asymmetric thermocline depth anomaly is always in the Sverdrup balance with the zonal wind stress anomaly.

The inclusion of both the zonally averaged and asymmetric parts of the thermocline depth variations allows us to investigate two important, yet totally different feedback processes, a negative feedback that diminishes original anomalies and causes a phase shift, and a positive feedback that magnifies and maintains the existing interannual anomalies. The former controls the up and down of the mean thermocline level across the basin whereas the latter represents the longitudinal slope or east–west seesaw of the thermocline depth anomalies. It turns out that a simple model of ENSO must incorporate both components of the thermocline depth variation.

The physical mechanism behind this stationary SST mode involves two essential types of feedback processes, as illustrated in Fig. 13. In the left side of this schematic diagram, it depicts a positive feedback cycle. Suppose we start from an initial phase of the El Niño, say, a weak warming in the eastern equatorial Pacific. In response to the SST forcing, the atmospheric east–west circulation, the reversed Walker circulation, is established, which further increases the SST anomaly through the following processes: 1) anomalous downwelling in the eastern equatorial Pacific that suppresses the mean upwelling and causes a positive time change rate for the SST; 2) anomalous zonal temperature advection that brings the warmer water from the west to the east; 3) the deepening of the thermocline depth in the eastern Pacific [according to Eq. (2.15b)] that further increases the subsurface temperature and warms SST. Because of the positive feedback processes, the El Niño develops. In the right side of Fig. 13, it depicts a negative feedback cycle through which an El Niño condition diminishes and a La Niña condition develops. The warming in the eastern equatorial Pacific intensifies the local Hadley circulation and strengthens the subtropical highs. The increase in the subtropical highs causes the intensification of easterly trades off the equator, which, together with equatorial wind forcing, excite a host of Rossby waves that carry opposite (relative to the equatorial ones) signals. The accumulated effect of those waves through their reflections in the western boundary slowly adjusts the zonal-mean thermocline depth at the equator. The intensified off-equatorial trades also induce
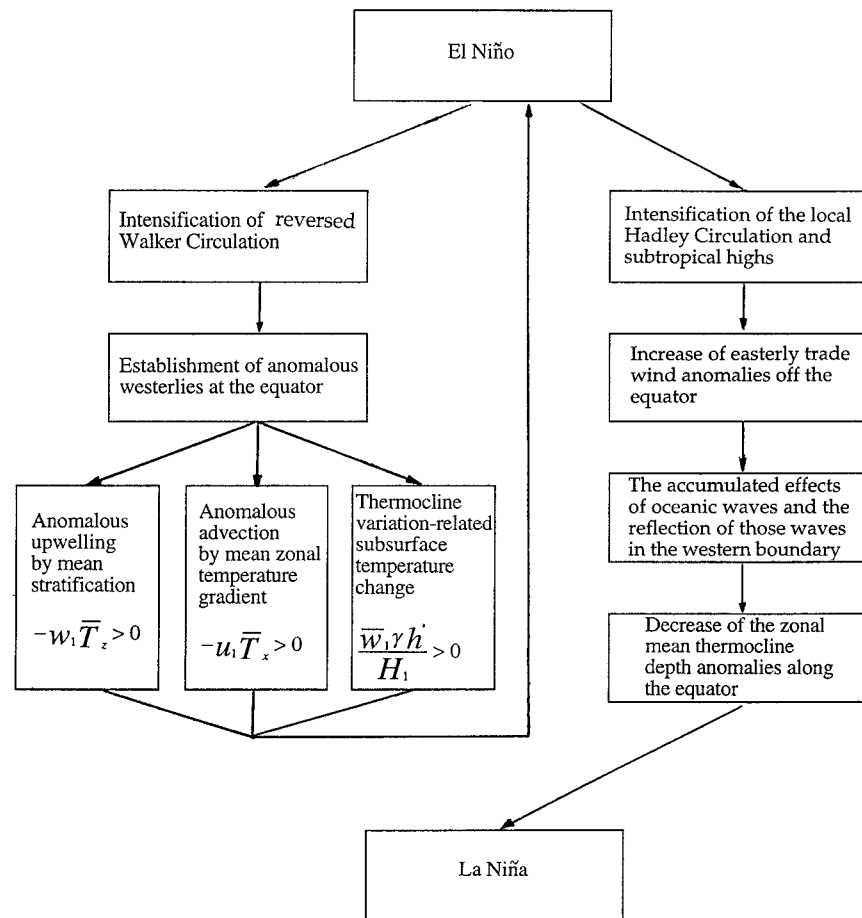
FIG. 13. A schematic diagram illustrating essential physics behind the conceptual ENSO dynamic model. The left side depicts a positive-feedback cycle that amplifies and maintains an interannual SST anomaly, whereas the right side depicts a negative feedback cycle that diminishes the original anomaly and promotes an opposite phase of the El Niño.

zonal-mean mass transport through the divergence at the equator of meridional currents in the upper ocean. Both effects cause a negative time change rate for the zonal-mean thermocline depth anomaly at the equator. The decrease of the whole thermocline layer at the equator eventually brings in a cold episode, the La Niña phase.

Figure 13 implies that whereas the equatorial east–west circulation, the Walker circulation, acts as a positive feedback factor to amplify and maintain an interannual anomaly, the Hadley circulation acts as a negative feedback factor and is responsible for the phase transition of ENSO. As pointed out by Nigam and Shen (1993) and Oort and Yienger (1996), from an observational point of view, the interannual variation in the Hadley cell is indeed strongly, inversely correlated with that of the Walker circulation. A direct response of the ocean to the Hadley circulation, through induced divergence (convergence) of meridional ocean currents, is expected to have a positive feedback impact on air–sea coupling, but it does not (as shown by our numerical

experiments) influence the phase transition. The indirect contribution of the Hadley circulation, through changing subtropical highs and off-equatorial zonal winds, on the other hand, is indeed important in resulting in the delayed response of the zonal-mean equatorial thermocline depth anomaly. McCreary (1983) first recognized the negative feedback effect by the Hadley cell, in an ideal fashion. The present study emphasizes the important contribution of the Hadley circulation to the phase transition of ENSO.

For a reasonable parameter regime, the interannual oscillation in the model has a period of 2–7 yr. In general, the growth rates and oscillation periods in the stationary SST mode depend on the width of the ocean basin, on the basic-state stratification and vertical motion, and on air–sea coupling strength. The stronger the basic-state upwelling and stratification, the larger the growth rates, and the shorter the oscillation period. The stationary SST mode is also seasonally dependent. A maximum (minimum) growth rate occurs in September (March), which may explain the frequent occurrence of

mature phases of the El Niño in the later part of the year and a rapid drop of lagged correlation of the Southern Oscillation index in the boreal spring.

The stationary SST mode is characterized by the zonal-mean thermocline depth anomaly leading the SST and wind anomalies. The exact phase lags depend on a number of factors, such as the basic state and coupling strength. It varies from a few months to more than a year. Such a phase relationship is found not only in our linear dynamic model, but also in a nonlinear model of Wang and Feng (1996), in the intermediate Cane-Zebiak type models (Zebiak and Cane 1987; Chang et al. 1995), and in the NCEP 4D data assimilation set (Fig. 3b).

In contrast to the stationary oscillation feature in the SST and wind fields, the thermocline depth anomaly (the sum of the zonally averaged and asymmetric components) "propagates" eastward along the equator. This agrees well with observations and coupled GCM simulations. The propagation results from the combined effects of the two different types of response of ocean thermocline to atmospheric wind forcing.

It is noted that a recent independent study by Jin (1997) proposed a very similar paradigm, the core of which is the nonequilibrium of the zonal-mean thermocline depth anomaly. The difference between the two studies lies in the mathematical derivation and physical interpretation of how this nonequilibrium is generated. Jin (1997) introduced a "symbolical" thermocline depth equation [his Eq. (2.2) or (2.3)] based on some physical arguments, whereas in the current model we derive both the zonal mean and zonally asymmetric thermocline depth anomaly equations [Eqs. (2.8) and (2.15)] based on reduced-gravity shallow water dynamics. Physically we emphasize the role of off-equatorial winds resulting from the Hadley circulation change in determining the phase transition.

A number of assumptions and simplifications have been made in the current model, among which are the specification of zonal, as well as meridional, structures of SST and wind anomalies and the symmetry, relative to the equator, of the interannual oscillation. By specifying the zonal profiles of the wind and SST anomalies (based on EOF analyses from observations), we intentionally filter out the zonally propagating SST mode. By considering the accumulated wave effects on the zonal-mean thermocline depth variations, we modify the original delayed oscillator mode. The specification of the Hermit-Gaussian meridional structure for zonal wind stress is a key to link the Hadley circulation to the Southern Oscillation. Many modifications or extensions can be made to improve the model physics and mathematical representations. For instance, a relaxation of the fixed zonal structure for the SST and wind can allow the model to include the zonally propagating SST mode discussed by Neelin (1991). The inclusion of nonlinearity in the model may allow us to discuss the chaos of interannual oscillations. One of the major limitations of the present model is the regularity of interannual oscillations. In fact, such regular oscillations are natural solutions for a linear, constant coefficient, second-order differential equation such as (3.1). Zebiak and Cane (1987) showed that an irregular oscillation may emerge when a seasonally varying basic state is introduced. Jin et al. (1994), Tziperman et al. (1994), and Chang et al. (1994) found that the irregularity of ENSO may result from chaotic behaviors of nonlinearity of coupled ocean–atmosphere system interacting with the seasonal cycle. The purpose of this study is not to explain the complex characteristics of ENSO, but rather to address a basic question, namely, what is the mechanism that determines the phase transition of ENSO. Whether the physics behind this conceptual model reflects the real world or whether it is essential to combine all possible mechanisms, the delayed oscillator and slow SST modes, for example, together is an open question. That deserves further observational and modeling studies.

REFERENCES

Anderson, D. L. T., and J. P. McCreary, 1985: Slowly propagating disturbances in a coupled ocean–atmosphere model. *J. Atmos. Sci.,* **42,** 615–629.

Battisti, D. S., and A. C. Hirst, 1989: Interannual variability in the tropical atmosphere–ocean system: Influence of the basic state and ocean geometry. *J. Atmos. Sci.,* **46,** 1678–1712.

Bjerknes, J., 1966: A possible response of the atmospheric Hadley circulation to equatorial anomalies of ocean temperature. *Tellus,* **18,** 820–829.

——, 1969: Atmospheric teleconnections from the equatorial Pacific. *Mon. Wea. Rev.,* **97,** 163–172.

Cane, M. A., 1979: The response of an equatorial ocean to simple wind stress patterns. Part I: Model formulation and analytic results. *J. Mar. Res.,* **37,** 233–252.

——, and S. E. Zebiak, 1985: A theory for El Niño and the Southern Oscillation. *Science,* **228,** 1084–1087.

Chang, P., B. Wang, T. Li, and L. Ji, 1994: Interactions between the seasonal cycle and ENSO: Frequency entrainment and chaos in a coupled atmosphere–ocean model. *Geophys. Res. Lett.,* **21,** 2817–2820.

——, L. Ji, B. Wang, and T. Li, 1995: On the interactions between the seasonal cycle and El Niño–Southern Oscillation in an intermediate coupled ocean–atmosphere model. *J. Atmos. Sci.,* **52,** 2353–2372.

Gill, A. E., 1985: Elements of coupled ocean–atmosphere models for the tropics. *Coupled Ocean-Atmosphere Models,* J. C. J. Nihoul, Ed., Elsevier Oceanogr. Ser., No. 40, 303–327.

Hirst, A. C., 1986: Unstable and damped equatorial modes in simple coupled ocean–atmosphere models. *J. Atmos. Sci.,* **43,** 606–630.

Ji, M., A. Leetmaa, and J. Derber, 1995: An ocean analysis system for seasonal to interannual climate studies. *Mon. Wea. Rev.,* **123,** 460–481.

Jin, F.-F., 1997: An equatorial ocean recharge paradigm for ENSO. Part I: conceptual model. *J. Atmos. Sci.,* **54,** 811–829.

——, J. D. Neelin, and M. Ghil, 1994: El Niño on the devil's staircase: Annual subharmonic steps to chaos. *Science,* **264,** 70–72.

Lau, K. M., 1981: Oscillations in a simple equatorial climate system. *J. Atmos. Sci.,* **38,** 248–261.

Lau, N. C., S. G. H. Philander, and M. J. Nath, 1992: Simulation of ENSO-like phenomena with a low-resolution coupled GCM of the global ocean and atmosphere. *J. Climate,* **5,** 284–307.

Li, B., and A. J. Clarke, 1994: An examination of some ENSO mechanisms using interannual sea level at the eastern and western equatorial boundaries and the zonal averaged wind. *J. Phys. Oceanogr.,* **24,** 681–690.

Li, T., and S. G. H. Philander, 1996: On the annual cycle of the eastern equatorial Pacific. *J. Climate,* **9,** 2986–2998.

Lindzen, R. S., and S. Nigam, 1987: On the role of sea surface temperature gradients in forcing low level winds and convergence in the tropics. *J. Atmos. Sci.,* **44,** 2418–2436.

McCreary, J. P., 1983: A model of tropical ocean–atmosphere interaction. *Mon. Wea. Rev.,* **111,** 370–387.

——, and D. L. T. Anderson, 1984: A simple model of El Niño and the Southern Oscillation. *Mon. Wea. Rev.,* **112,** 934–946.

Neelin, J. D., 1991: The slow sea surface temperature mode and the fast-wave limit: Analytic theory for tropical interannual oscillation and experiments in a hybrid coupled model. *J. Atmos. Sci.,* **48,** 584–606.

Nigam, S., and H.-S. Shen, 1993: Structure and oceanic and atmospheric low-frequency variability over the tropical Pacific and Indian Oceans. Part I: COADS observations. *J. Climate,* **6,** 657–676.

Oort, A. H., and J. J. Yienger, 1996: Observed variability in the Hadley Circulation and its connection to ENSO. *J. Climate,* **9,** 2751–2767.

Philander, S. G. H., 1990: *El Niño, La Niña, and the Southern Oscillation.* Academic Press, 293 pp.

——, and R. C. Pacanowski, 1981: The response of equatorial oceans to periodic forcing. *J. Geophys. Res.,* **86,** 1903–1916.

——, T. Yamagata, and R. C. Pacanowski, 1984: Unstable air–sea interaction in the tropics. *J. Atmos. Sci.,* **41,** 604–613.

——, R. C. Pacanowski, N. C. Lau, and M. J. Nath, 1992: Simulation of ENSO with a global atmospheric GCM coupled to a high-resolution, tropical Pacific Ocean GCM. *J. Climate,* **5,** 308–329.

Rasmusson, E. M., and T. H. Carpenter, 1982: Variations in tropical sea surface temperature and surface wind fields associated with the Southern Oscillation/El Niño. *Mon. Wea. Rev.,* **110,** 354–384.

Schneider, E. K., B. Huang, and J. Shukla, 1995: Ocean wave dynamics and El Niño. *J. Climate,* **8,** 2415–2439.

Schopf, P. S., and M. J. Suarez, 1988: Vacillations in a coupled ocean–atmosphere model. *J. Atmos. Sci.,* **45,** 549–566.

Suarez, M. J., and P. S. Schopf, 1988: A delayed action oscillator for ENSO. *J. Atmos. Sci.,* **45,** 3283–3287.

Tziperman, E., L. Stone, M. A. Cane, and H. Jarosh, 1994: El Niño chaos: Overlapping of resonances between the seasonal cycle and the Pacific ocean–atmosphere oscillator. *Science,* **264,** 72–74.

Wakata, Y., and E. S. Sarachik, 1991: Unstable coupled atmosphere–ocean basin models in the presence of a spatially varying basic state. *J. Atmos. Sci.,* **48,** 2060–2077.

Wang, B., 1995: Transition from a cold to a warm state of the El Niño–Southern Oscillation cycle. *Meteor. Atmos. Phys.,* **56,** 17–32.

——, and Z. Feng, 1996: Chaotic oscillations of tropical climate: A dynamic system theory for ENSO. *J. Atmos. Sci.,* **53,** 2786–2802.

Wang, C., and R. H. Weisberg, 1994: On the ''slow mode'' mechanism in ENSO-related coupled ocean–atmosphere models. *J. Climate,* **7,** 1657–1667.

Webster, J. P., and S. Yang, 1992: Monsoon and ENSO: Selectively interactive system. *Quart. J. Roy. Meteor. Soc.,* **118,** 877–926.

Xie, S.-P., A. Kubikawa, and K. Hanawa, 1989: Oscillations with two feedback processes in a coupled ocean–atmosphere model. *J. Climate,* **2,** 946–964.

Yamagata, T., 1985: Stability of a simple air–sea coupled model in the tropics. *Coupled Ocean-Atmosphere Models,* J. C. J. Nihoul, Ed., Elsevier Oceanogr. Ser., No. 40, 637–657.

Zebiak, S. E., and M. A. Cane, 1987: A model ENSO. *Mon. Wea. Rev.,* **115,** 2262–2278.